

pubs.acs.org/JACS Article

Modulation of Alzheimer's Disease A $oldsymbol{eta}$ 40 Fibril Polymorphism by the Small Heat Shock Protein $oldsymbol{lpha}$ B-Crystallin

- 3 Natalia Rodina, Simon Hornung, Riddhiman Sarkar, Saba Suladze, Carsten Peters, Philipp W. N. Schmid,
- ⁴ Zheng Niu, Martin Haslbeck, Johannes Buchner, Aphrodite Kapurniotu, and Bernd Reif*



Cite This: https://doi.org/10.1021/jacs.4c03504



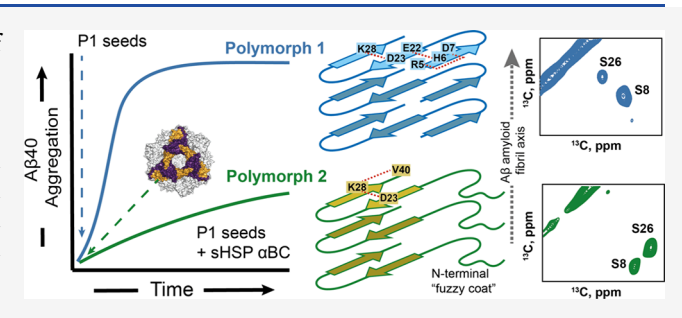
ACCESS

III Metrics & More

Article Recommendations

s Supporting Information

s **ABSTRACT:** Deposition of amyloid plaques in the brains of 6 Alzheimer's disease (AD) patients is a hallmark of the disease. AD 7 plaques consist primarily of the beta-amyloid ($A\beta$) peptide but can 8 contain other factors such as lipids, proteoglycans, and chaperones. 9 So far, it is unclear how the cellular environment modulates fibril 10 polymorphism and how differences in fibril structure affect cell 11 viability. The small heat-shock protein (sHSP) alpha-B-Crystallin 12 (α BC) is abundant in brains of AD patients, and colocalizes with 13 $A\beta$ amyloid plaques. Using solid-state NMR spectroscopy, we 14 show that the $A\beta$ 40 fibril seed structure is not replicated in the



15 presence of the sHSP. α BC prevents the generation of a compact fibril structure and leads to the formation of a new polymorph with 16 a dynamic N-terminus. We find that the N-terminal fuzzy coat and the stability of the C-terminal residues in the A β 40 fibril core 17 affect the chemical and thermodynamic stability of the fibrils and influence their seeding capacity. We believe that our results yield a 18 better understanding of how sHSP, such as α BC, that are part of the cellular environment, can affect fibril structures related to cell 19 degeneration in amyloid diseases.

■ INTRODUCTION

21 Aggregation of β -amyloid peptides (A β) into amyloid fibrils in 22 the brain tissue is one of the hallmarks of Alzheimer's disease. 1 23 Despite their general overall similarities, $A\beta$ fibrils are known 24 to be highly polymorphic.²⁻⁵ It is thought that differences in 25 fibril morphology have implications with regard to fibril-26 induced cellular cytotoxicity, and it has been shown that 27 certain Aeta aggregate morphologies are more toxic in 28 comparison to others.^{6,7} Recently, two structurally defined 29 Aeta polymorphs were shown to promote different pathological 30 changes in susceptible mice. The occurrence of distinct fibril 31 morphologies is a consequence of flat energy surface of the 32 protein misfolding landscape. 9,10 We show here that small 33 variations of the solution conditions can influence the 34 conversion into one or the other polymorphic structure. It is known that the cellular environment influences the 36 kinetics of fibril formation. For example, membranes modulate 37 amyloid fibril growth and can either accelerate or inhibit 38 aggregation. 11-14 Similarly, glycosaminoglycans such as hepar-39 an, keratan, or chondroitin sulfates induce an accelerated 40 conversion into amyloid fibril structures and amyloid 41 aggregates are found to be colocalized in the proteoglycan 42 matrix. 15-17 Finally, chaperones inhibit protein aggregation 43 and can rescue cells from the cytotoxic side effects of amyloid 44 aggregation. 18-22 Despite the fact that the cellular context has 45 a direct impact on the kinetics of amyloid formation, it is not 46 understood whether and in which way fibril morphology is changed and how the cellular environment triggers these 47 morphological changes. In this manuscript, we address the 48 question of whether and how the cellular environment can 49 affect amyloid fibril structure. As an example, we focus on the 50 small heat shock protein (sHSP) α B-Crystallin (α BC), which 51 is one of the most intriguing chaperones known to inhibit the 52 aggregation of various amyloidogenic proteins, including A β . 53 α BC is upregulated in Alzheimer's disease, dementia with 54 Lewy bodies and Parkinson's disease and is found to be 55 colocalized with the amyloid plaques of Alzheimer's 56 patients. ^{23,24} At the same time, it has been shown that α BC 57 modulates A β -induced cytotoxicity. ^{25–28}

Amyloid fibrils are formed via distinct mechanisms and 59 pathways such as primary nucleation, elongation, secondary 60 nucleation, fragmentation etc. Secondary nucleation was 61 found to be the major pathway for the generation of new $A\beta$ 62 amyloid fibrils in which nucleation of $A\beta$ peptide happens on 63 the surface of existing $A\beta$ fibrils. The role of secondary 64 nucleation in the structural polymorphism of fibrils is highly 65 debated. It was suggested that secondary nucleation is highly 66

Received: March 11, 2024 Revised: July 1, 2024 Accepted: July 2, 2024



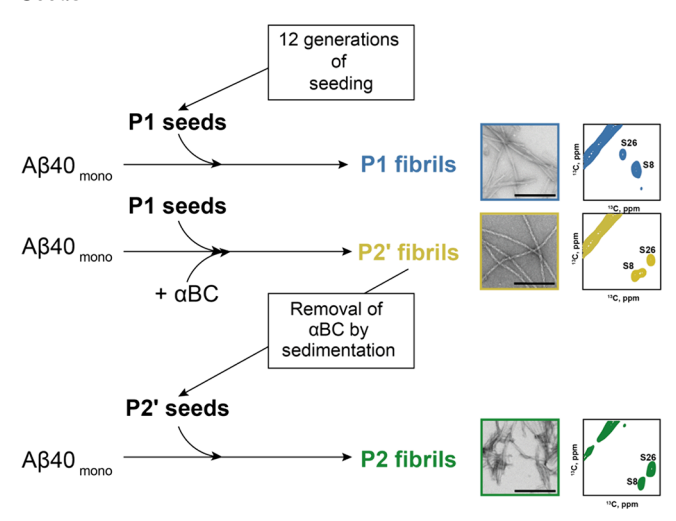
67 dependent on environmental conditions and can not ensure 68 the preservation of the seed structure in comparison to 69 elongation. 35-37 On the other hand, preservation of the 70 polymorph structure has been observed in secondary 71 nucleation dominated A β aggregation.³⁸ In this context, the 72 role of the so-called fibrillar fuzzy coat, i.e. the dynamic 73 residues in the protein sequence that are not part of the fibril 74 core, is not well understood. 39,40 Interestingly, secondary 75 nucleation and elongation in $A\beta$ aggregates occur at different 76 sites. 41 Inhibitors can thus differentially interfere with the 77 various aggregation pathways. For example, clusterin is capable 78 of suppressing elongation in A β fibrils, while Brichos was found 79 to inhibit secondary nucleation processes and prevent the 80 formation of toxic oligomers. Brichos can bind to $A\beta$ 42 81 fibrils and effectively prevent fibril-catalyzed nucleation even at 82 low concentrations. Hsp27 and Hsp70 inhibit elongation of 83 α -synuclein fibrils. DnaJB6 binds to A β 42 fibrils and 84 inhibits secondary nucleation. 46 α BC interacts with the mature 85 A β and α -synuclein fibrils and inhibits their elongation. ^{47–49} 86 αBC uses different interfaces to interact with amorphous or amyloid-forming substrates. 50 Amorphous clients bind to the 88 NTR of the sHSP while $A\beta$ fibrils interacts rather with the 89 edge groove (β 4/8) of α BC. Also α BC prevents aggregation at 90 substoichiometric concentrations. It has therefore been 91 hypothesized that αBC binds to fibril ends. It seems thus 92 plausible that the environment influences or even dictates the 93 fibril growth mechanism and redirects amyloids into a distinct 94 polymorphic structure.

In this manuscript, we show how αBC affects A β 40 fibril 96 polymorphism. Structural changes are probed using MAS 97 solid-state NMR. These experiments are complemented by biophysical assays in which the thermodynamic stability of 99 A β 40 fibril as well as their seeding competence is probed. In 100 addition, the effects of different fibril polymorphs on the 101 viability of cultured PC12 cells are determined using the MTT 102 reduction assay.

RESULTS AND DISCUSSION

 α BC Inhibits the Replication of the Seed Structure 105 and Leads to the Formation of a New A β 40 Polymorph. 106 To obtain reproducible and well-defined fibril structures, in 107 vitro seeded fibril preparations are employed (Scheme 1). 108 Without seeding, heterogeneous solid-state NMR spectra are 109 obtained that show various morphologies in TEM images 110 (Figure S1A,B). In particular, we used a protocol involving 12 111 generations of seeding carried out at 37 °C. ⁵¹ The A β 40 fibrils 112 obtained this way are referred to as fibril polymorph 1 (P1) in 113 this work. Although αBC does not seem to completely inhibit 114 fibril-catalyzed seeding, the chaperone induces a dramatic 115 reduction in the aggregation rate and yields a reduction of the 116 ThT plateau intensity (Figure 1A). The amount of insoluble 117 A β 40 fibrils is reduced and a fraction of A β 40 peptide remains 118 in solution (Figure S1E). At the same time, the presence of 119 α BC results in a change of fibril morphology as observed in 120 negative stain transmission electron microscopy (TEM) 121 images. This new polymorph is referred to as polymorph 2' 122 (P2') (Scheme 1) in the following. In the presence of α BC $[A\beta]: [\alpha BC] = 10:1$), P1-seeded fibrils appear more isolated, 124 and less clustered in comparison to the sample that was grown 125 with the chaperone (Figure 1C,D). We have used a molar 126 ration of $[A\beta]$: $[\alpha BC] = 10:1$, since this value corresponds best 127 to the physiological situation. The concentration of soluble $A\beta$ 128 in AD brain has been estimated to be in the range of 0.5 to 15

Scheme 1. Preparation of Different A β 40 Polymorphs and Seeds



^aP1 seeds were obtained using a protocol involving 12 generations of seeding, which starts from monomeric A β 40. The P1 fibril sample was obtained from monomeric 13 C, 15 N labeled A β 40 (50 μ M) in the presence of 5% P1 seeds. The P2' fibril sample was obtained from monomeric 13 C, 15 N labeled A β 40 (50 μ M) in the presence of 5% P1 seeds and 5 μM αBC . P2" fibrils from Figure S1(not shown in the scheme) were obtained from monomeric 13 C, 15 N labeled A β 40 (50 μ M) in the presence of 5% P1 seeds and 25 μ M α BC. Non-bound αBC was washed away from P2' fibrils via 5 subsequent rounds of sedimentation (21,000 rcf, 30 min). The pellet was resuspended and sonicated to be used as seeds (P2' seeds). The P2 fibril sample was obtained from monomeric ¹³C, ¹⁵¹³C, ¹⁵N labeled fibrils. The structure of P1 and P2 fibrils was validated using solid-state NMR. Snapshots of the TEM microphotographs of P1, P2' and P2 fibril from Figure 1C,D and Figure S2E, respectively are shown. The serine region indicates the different polymorphs from Figure 1E for P1 and P2', and from Figure 2D for P2 are shown.

ng per mg of tissue, i.e. (0.1-3.8) nM, while it is on the order 129 of 150 nM in the insoluble fraction. 52,53 At the same time, the 130 αBC concentration amounts to (140 \pm 30) ng per 1 mg of 131 tissue corresponding to a concentration of (7.0 ± 1.5) nM.⁵⁴ 132

In EM images, we observe a range of different diameters in 133 P1 fibrils with an average diameter of 14.3 \pm 2.2 nm. The P2' 134 fibrils formed in the presence of 5 μ M α BC appear to be 135 overall thinner with an average diameter of 10.2 ± 1.6 nm 136 (Figure 1B). To characterize the structural differences and 137 properties of the two fibril polymorphs, we prepared fibrils 138 from isotopically labeled A β 40 for NMR experiments by 139 seeding with P1 in the presence and absence of 5 μ M α BC 140 (Scheme 1). To appreciate the homogeneity of our 141 preparations, we recorded carbon-carbon correlation spectra 142 (50 ms mixing time DARR) for both samples. As expected, the 143 fibrils grown with the P1 seeds yield high-quality spectra that 144 contain a single set of NMR resonances (Figure 1E, blue 145 spectrum). Surprisingly, fibrils grown with P1 seeds in the 146 presence of 5 μ M α BC (molar ratio A β 40: α BC = 10:1) and 147 under otherwise identical conditions yield a different cross- 148 peak pattern (Figure 1E, yellow spectrum). Spectral differences 149 for the two preparations are easily identified by inspection of 150 e.g. the serine chemical shift region (highlighted with a red 151 square). The A β 40 sequence contains two serine residues (S8 152 and S26). For a homogeneous sample that comprises a single 153 polymorph, exactly two cross peaks should be observed. The 154

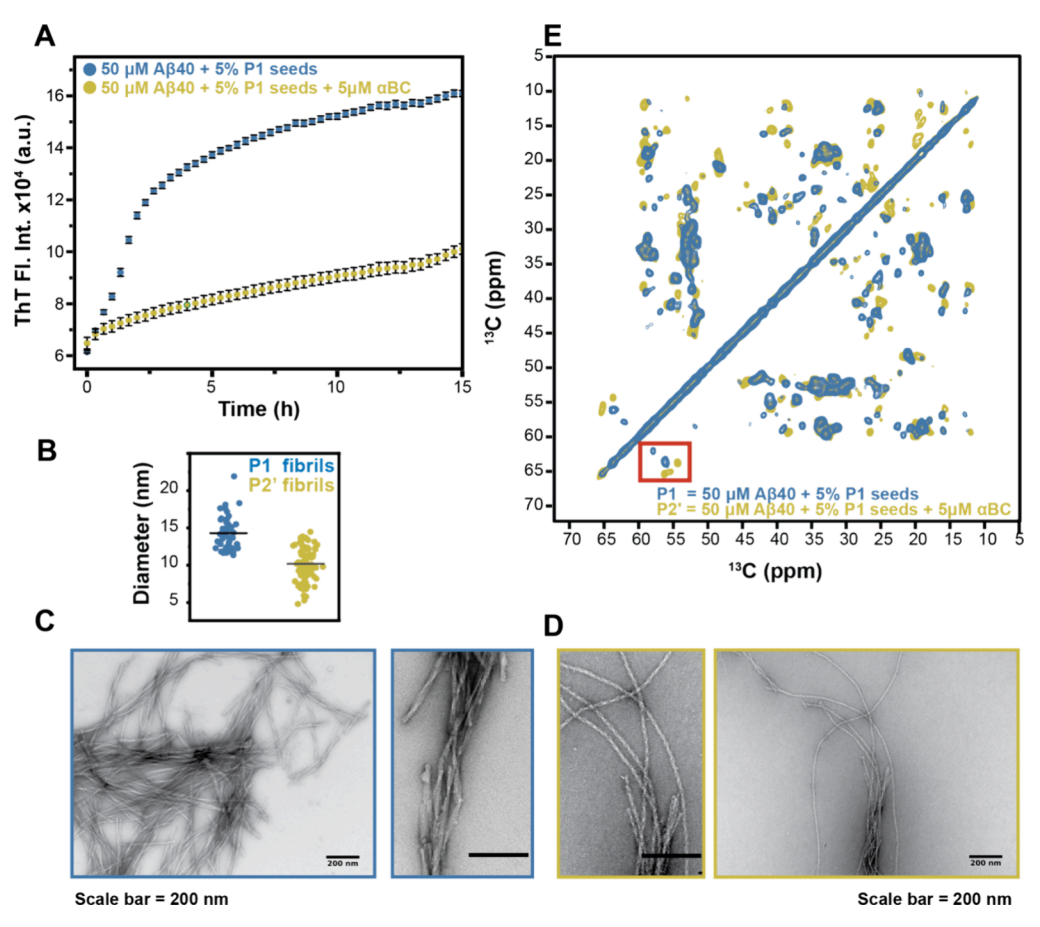


Figure 1. α BC affects seeded A β 40 fibril formation and structure. (A) ThT kinetic profile of seeded A β 40 aggregation in absence and presence of α BC. A concentration of 5 μ M α BC (yellow) has been employed in the experiment. Means (\pm SD) of one representative assay (n=3) with n=3 well each are shown. (B) Fibril diameter for polymorph P1 (blue) and P2' (yellow). The plot shows 50 (for P1) and 100 (for P2') independent measurements. The horizontal line indicates the mean value. (C) Representative TEM images of A β 40 fibrils grown using 5% P1 seeds in absence of 5 μ M α BC at two magnifications: 60 K on the right and 30 K on the left. (D) Representative TEM images of A β 40 fibrils grown using 5% P1 seeds in the presence of 5 μ M α BC at two magnifications: 60 K on the left and 30 K on the right. (E) Superposition of 2D- 13 C, 13 C MAS correlation spectra of A β 40 fibrils recorded for samples grown in absence (blue) and presence (yellow) of 5 μ M α BC. For all experiments, fibrils were grown using an initial 50 μ M monomeric A β 40 solution. To catalyze fibril formation, 5% P1 seeds have been employed.

155 differences in cross peak positions suggest that α BC induces a 156 structural change in the fibril morphology.

To verify the influence of αBC on the reproduction of the 158 seed structure, we prepared a second sample (P2") for which 159 isotopically labeled $A\beta 40$ was seeded with P1 fibrils in the 160 presence of a 5× higher concentration of the chaperone (25 161 μ M α BC) (Figure S1C,D). Under these conditions, the 162 amount of the produced fibrils is heavily reduced (Figure S1E), 163 and thus, the quality of the obtained NMR spectra decreases. 164 Still, the spectral fingerprint is reproduced, and the trend to 165 yield polymorph P2' is even increased under these conditions 166 (Figure S1C, pink spectrum).

Since a fraction of α BC remains bound to the P2' and P2" 168 fibrils after one round of sedimentation (Figure S1E), we 169 wanted to find out whether P2' morphology requires the 170 presence of the chaperone. For that purpose, several cycles of 171 subsequent sedimentations and resuspensions of the P2' 172 preparation were performed to separate A β 40 fibrils and 173 α BC. The obtained fibrils were subsequently sonicated and 174 employed as seeds (Scheme 1). Isotopically labeled A β 40 175 seeded with these P2' seeds resulted in the polymorph P2 176 (P2). 2D 13 C, 13 C correlation spectra of P2 fibrils are highly 177 homogeneous and match the spectra of the P2' preparation 178 (Figure S2A). Interestingly, although the DARR spectra look

almost identical and the secondary chemical shifts of P2 and 179 P2' fibrils are highly correlated (r=0.99) (Figure S2B,C), the 180 overall morphology observed in TEM looks different (Figure 181 S2E). However, the diameter of the individual fibril is 182 unchanged, and is on the order of (9.3 \pm 2.4) nm (Figure 183 S2E, inset). The observed differences are due to increased 184 clustering of fibrils which is presumably prevented by α BC in 185 the P2' preparation. In the following, we were aiming for a 186 more detailed structural characterization of the two A β 40 fibril 187 polymorphs P1 and P2 (Figure S2D). NMR chemical shift 188 assignments were obtained using 3D NCACX and NCOCX 189 experiments. Chemical shift assignments are deposited in the 190 BMRB under the access code 52337 and 52338, respectively. 191

P1 and the α BC-Induced Polymorph P2 Differ in the 192 Structural Order of the A β 40 N-Terminal Residues. To 193 get an estimate of the structural differences between the two 194 polymorphs, we compared the assignable residues in the two 195 preparations. In solid-state NMR experiments, only resonances 196 of rigid residues that are conformationally homogeneous can 197 be observed. While the assignment of P2 only starts from 198 amino acid R5 and has gaps until residue V18, residues D1 and 199 A2, together with amino acids R5 to G9 are observable in 200 polymorph P1 (Figure 2A). The analysis of the secondary 201 f2 chemical shifts reveals that both fibril polymorphs contain 3 β - 202

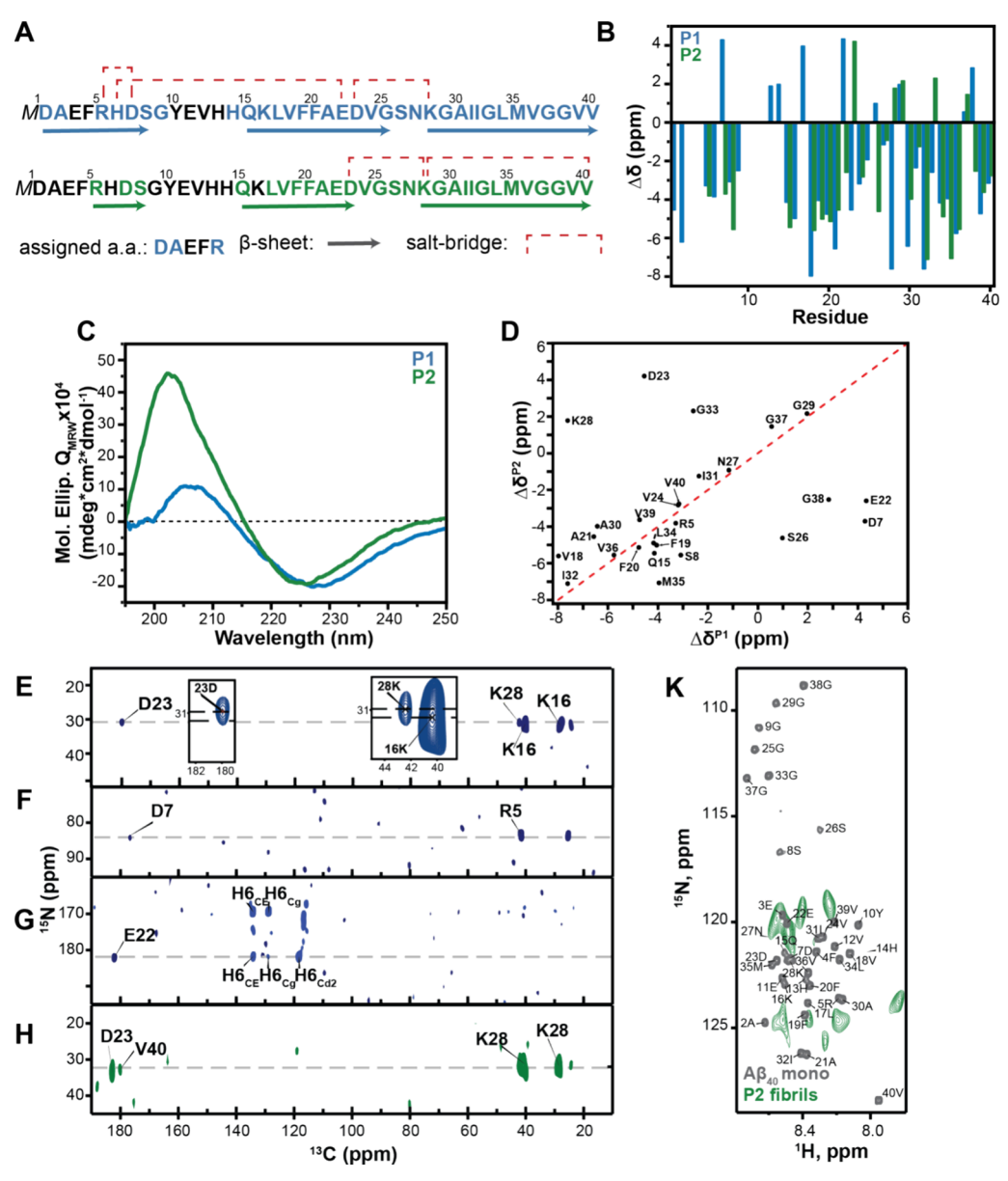


Figure 2. Structural characterization of the two $A\beta$ 40 fibrils polymorphs P1 and P2. (A) Amino acid sequence of $A\beta$ 40, with assigned residues and beta-sheet secondary structure elements for P1 (blue) and P2 (green). Experimentally observed salt-bridges are represented with red dashed lines. (B) Secondary chemical shifts $\Delta\delta$ for P1 and P2. The overall fibril topology is preserved in the two $A\beta$ 40 fibril polymorphs. (C) CD spectra for P1 and P2. The minimum indicative for β -sheet structure is shifted to higher wavelengths (229 nm instead of 225 nm), indicating a more compact structure. (D) Residue specific secondary chemical shift correlation plot. The *x*- and *y*- axis depict the experimental secondary chemical shifts for P1 and P2, respectively. Expect for residues D7, E22, D23, S26, K28 a high correlation coefficient is observed (r = 0.834). The secondary chemical shift is calculated as the differences between the experimentally observed chemical shift and the random coil chemical shift value. (E-G) 2D longrange TEDOR ¹³C, ¹⁵N correlation spectrum recorded for polymorph 1. The selected region shows the salt-bridge involving R5 and D7, K28 and D23, and H6 and E22, respectively. In panel (E), the inset shows that the salt bridge includes a correlation only between K28 and D23, while the ¹⁵N amino chemical shift of K16 does not match the correlation peak to D23. (H) 2D long-range TEDOR ¹³C, ¹⁵N correlation spectrum recorded for polymorph 2. The selected region shows two salt-bridges involving K28 and D23, K28 and V40. (I) Superposition of scalar coupling based ¹H, ¹⁵N correlation spectra for $A\beta$ 40 monomer in solution (gray) and P2 fibrils in the solid-state (green). The observed P2 chemical shifts are distinct from the resonances obtained in solution suggesting that the chemical environment for flexible residues in the N-terminus of the fibrils is affected by the core. INEPT based correlation spectra recorded for P1 fibrils yield no cross peaks.

203 sheets, however, in the P2 polymorph, the N-terminal β -sheet 204 is truncated compared to P1 (Figure 2A,B). The observed 205 differences between P1 and P2 in NMR chemical shift analysis 206 are accompanied with differences in their secondary structure 207 observed by CD spectroscopy (Figure 2C). In CD we observe 208 a shift of the minimum to larger wavelengths for P1 in 209 comparison to P2 fibrils which could be due to a better-defined 210 structure. The secondary chemical shifts of P1 and P2 fibrils

are rather similar, with the exception of D7, S8, A21, E22, D23, 211 K28, G33, M35 and G38. The chemical shift correlation plot 212 indicates that these residues are off the diagonal (Figure 2D), 213 suggesting that these residues are key elements that determine 214 the fibril topology and polymorphism.

It has been shown that salt bridges affect fibril poly- 216 morphism by stabilizing intermolecular interactions in the 217 fibril. To better characterize salt bridges in P1 and P2 fibrils, 218

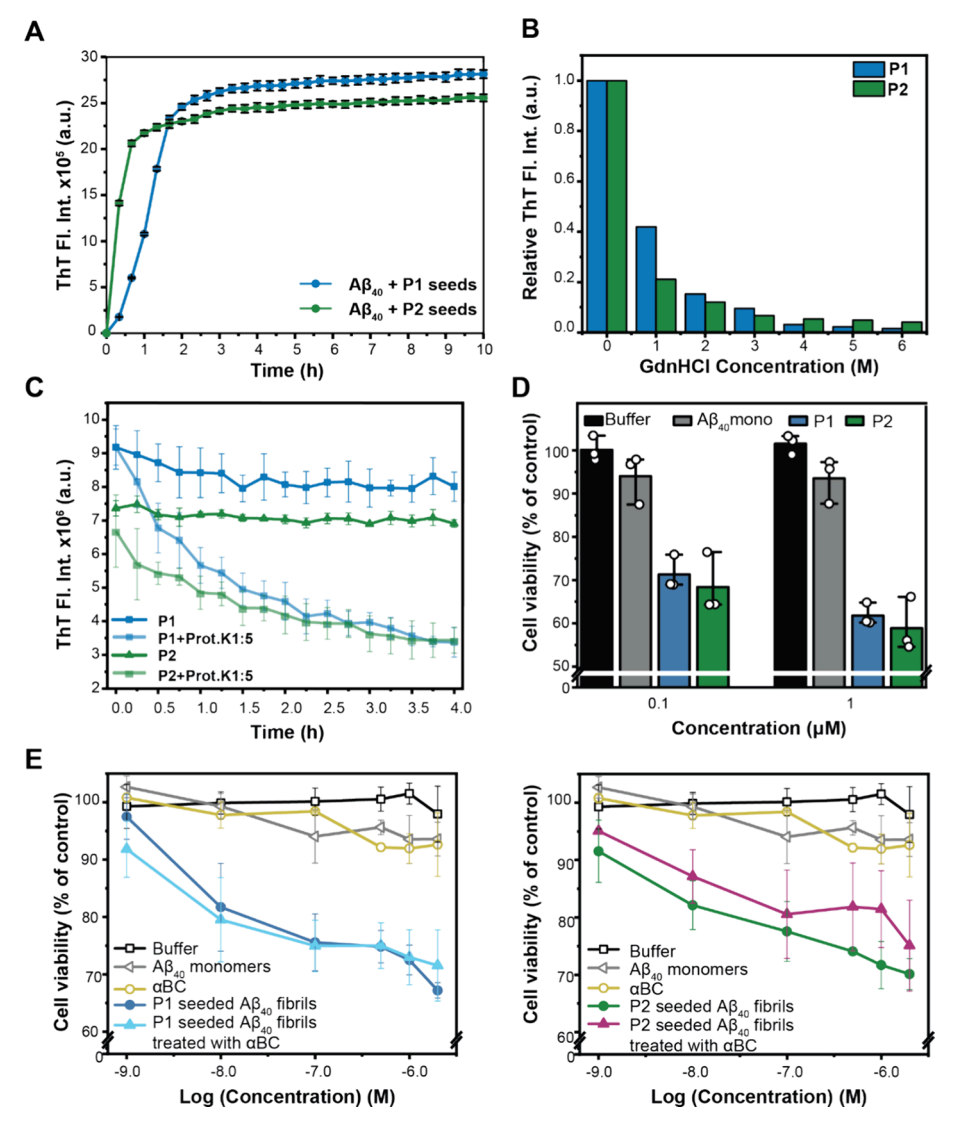


Figure 3. Functional characterization of A β 40 fibril polymorphs P1 and P2. (A) ThT aggregation profile of seeded A β growth using P1 (blue) and P2 (green) seeds, respectively. P1 seeds catalyze fibril formation more efficiently, while P2 seeds yield a sigmoidal seeding kinetics which is characteristic for an activated growth mechanism. The experiment was performed in triplicates. Averaged data is shown. The error bar reflects the standard deviation for the ThT fluorescence values of the triplicates at each time point. (B) GdnHCl disaggregation assay. Representative normalized ThT fluorescence intensity from 2 assays is represented as a function of the GdnHCl concentration. At low GdnHCl concentrations, P1 fibrils are more resistant to chemical denaturation, while at high GdnHCl concentrations P2 fibrils are more stable. (C) Proteinase K digestion assay to probe the stability of A β 40 fibril polymorph 1 (blue) and polymorph 2 (green). Not normalized ThT fluorescence intensity in absence (dark blue/green) and presence of proteinase K (light blue/green) is represented. A molar ratio [proteinase K]: $[A\beta 40] = 1:5$ has been used in the experiment. The experiment was performed in triplicates. Averaged data is shown. The standard deviation for the fluorescence values of the triplicates is shown as error bars. The normalized data shown in Figure S4A. (D) Cell viability of cultured PC12 cells after treatment with 0.1 µM and 1 μM Aβ40 fibril polymorph 1 (blue) or polymorph 2 (green) determined by MTT reduction assay. The viability of PC12 cells treated with buffer and A β 40 are shown as controls. Data are shown as means (\pm SD), 3 assays with n=3 wells each. The individual assays 1–3 are shown in Figure S4C. (E) Cell viability of cultured PC12 cells after treatment with A β 40 fibrils seeded with P1 (left) or P2 (right). Mature P1 and P2 seeded fibrils were incubated with 5 μ M α BC for 1 h prior to the MTT reduction assay. The viability of PC12 cells treated with buffer, α BC and freshly dissolved A β 40 monomers are shown as controls. Data are shown as means (\pm SD) of 2 (for fibrils with and without treatment with α BC and for α BC alone) or 3 (for buffer and A β 40 monomers) assays with n=3 wells each). For clarity, data for P1 and P2 seeded fibrils are shown separately in the left and right panels, respectively.

219 we implemented TEDOR solid-state NMR experiments. We 220 observe three distinct salt-bridges for polymorph P1, in 221 particular, H6-E22, D23-K28 and within the N-terminal 222 residues of A β 40 involving R5-D7 (Figure 2E-G). The R5-223 D7 and H6-E22 salt-bridges presumably contribute to the 224 increased stability and the loss of flexibility of the N-terminal 225 residues (1–10) in the P1 fibril polymorph. In the P2 226 polymorph, the characteristic salt-bridge D23-K28 is present,

which is found in most A β 40 fibril structures, while the salt- $_{227}$ bridges involving the N-terminus are missing. By contrast, we $_{228}$ find a second salt-bridge between K28 and V40 that potentially $_{230}$ in P2 fibrils (Figure 2H). We assume that this salt-bridge has a $_{231}$ similar structural function as the characteristic K28-A42 salt- $_{232}$ bridge found in A β 42 fibrils or the K28–V40 salt-bridge found $_{233}$ in the A β 40 "Iowa" mutant. $_{57,58}$ For P2, the cross peak $_{234}$

235 representing the D23-K28 salt-bridge is very weak in 236 comparison to P1 (Figure S3A,B), suggesting that the salt 237 bridge interaction in P2 is presumably dynamic. Although P1 238 and P2 share a similar fibril core structure, the two polymorphs 239 differ in the flexibility of the N- and C-terminal regions. To 240 further characterize differences in dynamics between P1 and 241 P2 fibrils, we recorded INEPT based experiments (Figure 2K 242 and Figure S3C). P1 fibrils do not yield any resonances in case 243 scalar coupling-based transfer elements are employed, 244 suggesting that the structure does not contain dynamic 245 residues (Figure S3C, blue). At the same time, P2 fibrils 246 yield a few weak INEPT cross peaks. For P1 and P2 fibrils, the 247 core parts (17-40) are highly similar. Both fibrils contain a 248 loop region involving residues 10-14. We do not expect any 249 INEPT resonances from these loop residues since dynamics in 250 this region is restricted due to the neighboring β -sheets. The 251 appearance of INEPT resonances in P2 fibrils must thus be due 252 to the dynamic N-terminal region. The ¹H, ¹⁵N correlation 253 spectra for monomeric A β 40 in solution and P2 fibrils in the 254 solid state are unlike, suggesting that the chemical environ-255 ments are distinct. The overall sensitivity of the INEPT based 256 experiments prevents the identification of individual amino acids and a sequential assignment.

The role of the flexible parts of the fibrillar structure was 259 neglected for many years. However, recently it became evident 260 that the so-called "fuzzy coat" of the fibrils plays a crucial role 261 in the process of fibril formation (especially elongation and 262 secondary nucleation), and is an important driving force for 263 intermolecular interactions, e.g. with membranes, mRNA and 264 chaperones. 37,59,60 The cryo-EM structures of A β 42 filaments 265 from human brains in familial AD have an extended fuzzy coat 266 (residues 1-11) compared to the filaments found in sporadic 267 AD (residues 1-8) and differ as well in the packing of the 268 protofilament.⁶¹ A detailed comparison of these polymorphs 269 suggests that G33 and G38 are involved in an interaction with 270 the N-terminus fuzzy coat that shields the hydrophobic C-271 terminus from the solvent. 62 Our experimental results indicate 272 that P1 fibrils lack this N-terminal fuzzy coat, which potentially 273 has consequences for the interactions of fibrils with their 274 environment.

In our experiments, both P1 and P2 polymorphs can be reproduced via seeding through a secondary nucleation-dominated mechanism (Figure 3A). Similarly, unseeded R β 40 monomers prepared under identical conditions fibrillize following a secondary nucleation mechanism (Figure S1D). At the same time, as already mentioned before, solid-state NMR shows that the resulting fibrils are heterogeneous (Figure S1A). Surprisingly, only 2 sets of serine peaks corresponding to P1 and P2 could be identified. This implies that both structures that be induced and are consistent with the environmental conditions.

The seeded ThT aggregation kinetics in the presence of 287 α BC implies that 49 fibrils rather grow by an elongation- 288 dominated mechanism. It is assumed that different sites in 49 aggregates are responsible for secondary nucleation and 290 elongation. The question of the role of the environment 291 and its influence on the fibril structure is, however, still 292 debated. While the Buell group suggests that elongation 293 preserves the seed structure, Linse and co-workers have shown 294 that 49 42 fibril strain characteristics can be efferently 295 propagated in secondary nucleation-dominated sysgetems. The presence of the chaperone, although the solvent and

aggregation conditions are identical. The absence of the lag- 298 phase in the seeded aggregation experiments in the presence of 299 the sHSP indicates that the chaperone does not completely 300 inhibit seeding (Figure 1A and Figure S1D). The action of 301 α BC prevents the generation of a compact fibril structure and 302 the conversion of the full amino acid sequence into an amyloid 303 fibril. The appearance of a new polymorph with a dynamic N- 304 terminus in the presence of α BC seems to indicate that the 305 chaperone directly interacts and destabilizes the A β 40 N- 306 terminal residues in the fibril structure and changes the 307 microenvironment in the nucleation process, resulting in a loss 308 of preservation of the fibril structure.

Increased Flexibility of the N-Terminus Leads to 310 Changes in Fibril Stability and Seeding Properties. 311 Amyloid fibrils are known to be polymorphic, but a link 312 between the fibril structure and its cellular properties is yet to 313 be identified. Obviously, differences in fibril structure have a 314 direct impact on the respective protein misfolding disease and 315 their progression. Initially, it was believed that bypassing 316 primary nucleation through seeding allows to replicate the seed 317 structure. 66-68 However, the ability of mature fibrils to act as 318 seeds and templates for the propagation of their structure can 319 differ significantly. E.g., it has been shown recently that *ex vivo* 320 fibril material extracted from patients is often incapable to 321 template and propagate its structure *in vitro*. 5,69,70

To better understand the fibril polymorph properties, we 323 tested the capacity of the different polymorphs to act as seeds. 324 In particular, we addressed the question of how efficiently the 325 different polymorphs are able to propagate their structures. 326 Our solid-state NMR experiments showed that both 327 polymorphs P1 and P2 can reproduce their structures upon 328 seeding (Figure S2D). In ThT experiments, we find that P2 329 seeds are able to catalyze A β 40 fibril formation faster and more 330 efficiently in comparison to P1 seeds (Figure 3A). In both 331 experiments, the same amount of seeds has been employed. 332 We hypothesize that the proper arrangement of the A β 40 N- 333 terminus in the P1 amyloid fibril is time-limiting in the fibril 334 growth kinetics. Interestingly, seeding with P1 or P2 using the 335 same concentration of A β 40 monomer results in a higher ThT 336 plateau fluorescence intensity for the P1 seeded fibrils. A high 337 ThT fluorescence quantum yield is related to the inhibition of 338 rotations around the bond connecting the benzothiazole and 339 benzylamine rings of the molecule. 71–73 It was suggested, that 340 clustering of fibrils results in additional binding sites with a 341 higher fluorescence quantum yield. In these studies, the 342 CD spectra of the insulin fibrils showed a red wavelength shift 343 compared to the lysozyme fibrils which suggested a correlation 344 between clustering of individual fibrils and ThT binding. A 345 higher fluorescence intensity in P1 fibrils could thus be a 346 consequence of an increased rigidity of ThT in the bound state 347 due to fibril clustering or might result from an enlarged 348 number of binding sites (such as β -sheet structures) in the 349 ordered N-terminus of the P1 fibrils.

Next, we examined the chemical stability of the two fibril 351 polymorphs to better understand the fibril properties. Using 352 ThT fluorescence as a read-out, we compared the stability of 353 P1 and P2 fibrils in the presence of different amounts of 354 GdnHCl (Figure 3B). We find that P2 fibrils are less stable 355 when treated with small amounts of GdnHCl (up to 3 M). 356 ThT is considered to specifically interact with β -sheet 357 structures and binds to fibril grooves. 77,78 In P2 fibrils, the β - 358 sheet core seems easier accessible for GdnHCl due to the 359 solvent accessible N-terminal fuzzy-coat. In the P1 fibrils, the 360

361 core structure appears to be better protected from chemical 362 degradation as the GdnHCl has to dissolve first the more 363 stable fibril surface. At high GdnHCl concentrations (4-6 M), 364 however, P1 looses its structure more quickly in comparison to 365 P2. We hypothesize that the $A\beta$ 40 N-terminus is already 366 dissolved under these conditions, and GdnHCl starts to attack 367 the C-terminal part of the fibril core. In P2 fibrils, the C-368 terminal region is stabilized by the extra salt-bridge between 369 K28 and V40, which inhibits further degradation. Our findings 370 are in good agreement with a recent computational study of 371 the Vendruscolo group on two types of human brain-derived 372 $A\beta$ 42 fibril polymorphs which show that the fuzzy coat 373 increases the overall solubility of the cross- β core of the 374 filaments. 62

Similar effects are observed in proteinase K stability assays. Although, as discussed earlier, the initial absolute ThT fluorescence differs for the two polymorphs (for the same concentration of fibrils), the ThT fluorescence plateau value are after treatment with proteinase K is identical for the two polymorphs (Figure 3C). This suggests that proteinase K is able to digest the different polymorphs to the exact same final amount. At the same time, inspection of the normalized curves (Figure S4A) and effects of different $[A\beta40]$:[Proteinase K] against enzymatic degradation in the first 15 min of treatment. However, after the initial 15 min, P1 fibrils rapidly lose ThT fluorescence intensity.

Many factors affect the cytotoxicity of amyloid fibrils. In 389 addition to the topology of the protofilament, the oligomeric 390 arrangement of the protofilaments in the mature fibrils as well 391 as the fibril length matter. ^{79–82} We find that the two 392 polymorphs have similar toxic effects on cultivated PC12 393 cells (Figure 3D and Figure S4C). The fibril structure and 394 especially intramolecular interactions have been shown to be 395 crucial for A β 40 fibril induced neuronal cytotoxicity. ^{83,84} Korn 396 et al. have shown that the cytotoxicity of A β 40 fibrils depends 397 on the contact between F19 and L34. We performed CHHC 398 and proton assisted recoupling (PAR) solid-state NMR 399 experiments with various mixing times in order to get 400 information about long-range contacts. Although we could 401 identify the F19 spin-systems in the aromatic region of the 50 402 ms dipolar assisted rotational resonance (DARR) spectrum of 403 P1, we did not observe any cross peaks to L34 in the 250 ms 404 CHHC experiment (Figure S3C). We were not able to assign 405 any carbon atoms of the F19 ring in the 50 ms DARR 406 spectrum recorded for P2 (Figure S3D). We assume that the 407 contact between L34 and a phenylalanine residue in the 408 amyloid hydrophobic core is too dynamic in our preparations. 409 Korn et al. lyophilized their fibril preparation before packing it 410 into the MAS solid-state NMR rotor. Removal of excess 411 solvent might allow to reduce dynamics and stabilize the fibril 412 structure. Fibrils are maintained in an aqueous environment 413 inside the rotor in our preparations by sedimenting the sample 414 directly into the MAS rotor. The preparation procedure might 415 thus explain these differences in the spectra.

To further investigate the role of the N-terminal fuzzy coat 417 on cell viability and interaction with α BC, we incubated 418 mature fibrils with the sHSP. Our results indicate that 419 treatment of mature P1 fibrils with α BC does not influence 420 their effects on PC12 cell viability, while P2 fibrils that were 421 treated with the same amount of chaperone show a somewhat 422 reduced cell-damaging effect (Figure 3E). The effect on cell 423 viability upon α BC treatment of mature P2 fibrils suggests that

interaction of the chaperone with the N-terminal fuzzy coat, 424 which might be responsible for cell penetration and cell 425 membrane disruption, might affect fibril toxicity. P1-induced 426 cytotoxicity is less affected by the chaperone due to the lack of 427 the fuzzy coat. Electrostatic interactions, along with specific 428 interactions with various cell receptors such as integrin, were 429 suggested to play an important role in the interaction of A β 430 with cell membranes. 85–88 Various experiments with deletions 431 and mutations in the N-terminus verified that the N-terminus 432 plays not only an important role in $A\beta$ fibrillation but also 433 impacts on cellular toxicity. 89,90 In Narayanan et al., we have 434 speculated that the ${\rm A}\beta$ aromatic hydrophobic core region 435 contributes mostly to the interaction with αBC . In the 436 analysis of the saturation transfer difference NMR spectrosco- 437 py (STD) experiments, however, a potential shift of 438 equilibrium between different A β aggregation states induced 439 by αBC has not been taken into account.

Oligomer-induced cytotoxic effects have been suggested to 441 be highly relevant for disease pathogenesis as well. 92 442 Nevertheless, the effects of fibril formation in the cell and 443 the consequences on cell fate cannot be neglected. $^{93-96}$ Cells 444 have evolved mechanisms that allow either to degrade fibrils or 445 to reduce the consequences of their presence in organs and 446 tissues. 30,97,98 Chaperones not only play an important role in 447 preventing aggregation of amyloidogenic proteins and 448 modulate fibril polymorphism but, as we know, interact with 449 mature fibrils. 43,47,48 Recently, disaggregases have been 450 discovered that are capable to unfold and solubilize amyloid 451 fibrils. All disaggregase machineries known so far such as 452 Hsp104, Hsp40 + Hsp70 + Hsp110, HtrA1 etc. are ATP- 453 dependent. 30,99,100 Even though that α BC is not a disaggregase 454 and not capable of disassembling an amyloid fibril, small heat 455 shock proteins such human Hsp27 and yeast Hsp26 seem to be 456 able to affect the fibrillar structure and cytotoxicity. 101,102

It was shown that α BC and CHIP interact with α -synuclein 458 and bind to its unstructured C-terminal domain. 103 As a 459 consequence, fibril uptake by the cell is diminished. A recent 460 study by Stepananko et al. showed that lphaBC treatment changes 461 fibril morphology and hints toward degradation of lysozyme 462 and β 2-microglobulin amyloid fibrils. Although there is 463 no detailed data on possible disaggregation of amyloid fibrils 464 by αBC , a lot of evidence suggests that the chaperone binds to 465 mature fibrils. 47-49 One possible mechanism of amyloid- 466 induced cytotoxicity is membrane disruption by shedding of 467 membrane-active oligomers. 106,107 Tipping et al. demonstrated 468 that chemical cross-linking of β 2-microglobulin fibrils with 469 Hsp70 increases the fibril stability and, this way, inhibits 470 leakage of toxic oligomers that cause membrane disruption and 471 cellular dysfunction. In this sense, interactions of αBC with the 472 N-terminal fuzzy coat of P2 might stabilize the amyloid fibril 473 structure and shift the equilibrium from the oligomer to a less 474 toxic fibril state.

CONCLUSIONS

We have shown that the small heat shock protein αBC inhibits 477 propagation of the $A\beta$ 40 fibril seed structure and induces the 478 formation of a new fibril polymorph. This polymorph is 479 characterized by a flexible N-terminus and is able to transmit 480 its structure even in the absence of the chaperone. The N- 481 terminal fuzzy coat of the αBC induced fibril polymorph (P2) 482 increases the seeding efficiency and at the same time yields a 483 decrease in the chemical stability at low GdnHCl concen- 484 trations. P2 is characterized by a stabilized amyloid core 485

476

543

558

559

560

561

562

572

486 structure which is a consequence of an additional salt-bridge at 487 the C-terminus of the peptide. Although the two polymorphs 488 show similar cytotoxic effects on PC12 cells, P2 induced 489 cytotoxicity seems to be reduced in the presence of α BC. We 490 suggest that the N-terminus of A β 40 is a key region not only 491 for peptide aggregation but for its interaction with sHSPs as 492 well. Our study sheds light on the molecular origin of fibril 493 polymorphism and contributes to the understanding of the 494 fibril fuzzy coat and its interactions with the cellular 495 environment.

ASSOCIATED CONTENT

Supporting Information

498 The Supporting Information is available free of charge at 499 https://pubs.acs.org/doi/10.1021/jacs.4c03504.

Description of the experimental procedures, materials and methods; NMR spectra of nonseeded fibril preparation, P1, P2', P2" and P2 fibrils; comparative analysis of P2 and P2' chemical shifts; TEM images of P2 fibrils; long-range contacts in P1 and P2 fibrils; ThT aggregation assay; Proteinase K stability assay; MTT assay (PDF)

AUTHOR INFORMATION

508 Corresponding Author

Bernd Reif - Bayerisches NMR Zentrum (BNMRZ) at the 509 Department of Biosciences, School of Natural Sciences, 510 Technische Universität München, Garching 85747, Germany; 511 Helmholtz-Zentrum München (HMGU), Deutsches 512 Forschungszentrum für Gesundheit und Umwelt, Institute of 513 Structural Biology (STB), Neuherberg 85764, Germany; 514 orcid.org/0000-0001-7368-7198; Email: reif@tum.de 515

516 Authors

525

526

527

528

529

530

531

532

533

534

535

536

537

538

539

540

541

542

500

501

502

503

504

505

506

Natalia Rodina – Bayerisches NMR Zentrum (BNMRZ) at 517 the Department of Biosciences, School of Natural Sciences, 518 Technische Universität München, Garching 85747, Germany; 519 Helmholtz-Zentrum München (HMGU), Deutsches 520 Forschungszentrum für Gesundheit und Umwelt, Institute of 521 Structural Biology (STB), Neuherberg 85764, Germany; 522 orcid.org/0000-0001-5860-7014 523 524

Simon Hornung - Division of Peptide Biochemistry, TUM School of Life Sciences, Technical University of Munich, Freising 85354, Germany; orcid.org/0000-0001-8338-2232

Riddhiman Sarkar – Bayerisches NMR Zentrum (BNMRZ) at the Department of Biosciences, School of Natural Sciences, Technische Universität München, Garching 85747, Germany; Helmholtz-Zentrum München (HMGU), Deutsches Forschungszentrum für Gesundheit und Umwelt, Institute of Structural Biology (STB), Neuherberg 85764, Germany; orcid.org/0000-0001-9055-7897

Saba Suladze – Bayerisches NMR Zentrum (BNMRZ) at the Department of Biosciences, School of Natural Sciences, Technische Universität München, Garching 85747, Germany; o orcid.org/0000-0001-6226-1570

Carsten Peters - Center for Functional Protein Assemblies (CPA), Department of Biosciences, Technische Universität München, Garching 85747, Germany; o orcid.org/0000-0002-7193-499X

Philipp W. N. Schmid – Center for Functional Protein Assemblies (CPA), Department of Biosciences, Technische 544 Universität München, Garching 85747, Germany 545 Zheng Niu - School of Pharmacy, Henan University, Kaifeng, 546 Henan 475004, China; o orcid.org/0000-0002-0965-8795 547 Martin Haslbeck - Center for Functional Protein Assemblies 548 (CPA), Department of Biosciences, Technische Universität München, Garching 85747, Germany; o orcid.org/0000-550 0001-6709-1240 551 Johannes Buchner - Center for Functional Protein Assemblies 552 (CPA), Department of Biosciences, Technische Universität 553 München, Garching 85747, Germany 554 Aphrodite Kapurniotu - Division of Peptide Biochemistry, 555 TUM School of Life Sciences, Technical University of Munich, 556 Freising 85354, Germany; orcid.org/0000-0001-6124-

Complete contact information is available at: https://pubs.acs.org/10.1021/jacs.4c03504

The authors declare no competing financial interest.

ACKNOWLEDGMENTS

This work was supported by the SFB 1035 (German Research 564 Foundation DFG, Sonderforschungsbereich 1035, projects 565 A06, B06, B07). We acknowledge NMR spectrometer time 566 at the Bavarian NMR Center (http://www.bnmrz.org). We are 567 grateful to Melina Daniilidis for the ESI-MS experiments to 568 verify the purity of the recombinant A β 40 peptide. We 569 acknowledge financial support from the Helmholtz-Gemein- 570 schaft. 571

REFERENCES

- (1) Tanzi, R. E.; Bertram, L. Twenty years of the Alzheimer's disease 573 amyloid hypothesis: a genetic perspective. Cell 2005, 120 (4), 545-574
- (2) Bertini, I.; Gonnelli, L.; Luchinat, C.; Mao, J.; Nesi, A. A new 576 structural model of A β 40 fibrils. J. Am. Chem. Soc. **2011**, 133 (40), 577 16013-22. 578
- (3) Lu, J. X.; Qiang, W.; Yau, W. M.; Schwieters, C. D.; Meredith, S. 579 C.; Tycko, R. Molecular structure of β -amyloid fibrils in Alzheimer's 580 disease brain tissue. Cell 2013, 154 (6), 1257-68. 581
- (4) Tycko, R. Physical and structural basis for polymorphism in 582 amyloid fibrils. Protein Sci. 2014, 23 (11), 1528-39.
- (5) Kollmer, M.; Close, W.; Funk, L.; Rasmussen, J.; Bsoul, A.; 584 Schierhorn, A.; Schmidt, M.; Sigurdson, C. J.; Jucker, M.; Fändrich, 585 M. Cryo-EM structure and polymorphism of A β amyloid fibrils 586 purified from Alzheimer's brain tissue. Nat. Commun. 2019, 10 (1), 587
- (6) Tycko, R. Amyloid polymorphism: structural basis and 589 neurobiological relevance. Neuron 2015, 86 (3), 632-45.
- (7) Petkova, A. T.; Leapman, R. D.; Guo, Z.; Yau, W. M.; Mattson, 591 M. P.; Tycko, R. Self-propagating, molecular-level polymorphism in 592 Alzheimer's beta-amyloid fibrils. Science 2005, 307 (5707), 262-5. 593
- (8) Gomez-Gutierrez, R.; Ghosh, U.; Yau, W.; Gamez, N.; Do, K.; 594 Kramm, C.; Shirani, H.; Vegas-Gomez, L.; Schulz, J.; Moreno- 595 Gonzalez, I.; Gutierrez, A.; Nilsson, K. P. R.; Tycko, R.; Soto, C.; 596 Morales, R. Two structurally defined $A\beta$ polymorphs promote 597 different pathological changes in susceptible mice. EMBO Rep. 598 **2023**, 24 (8), No. e57003.
- (9) Hartl, F. U.; Hayer-Hartl, M. Converging concepts of protein 600 folding in vitro and in vivo. Nat. Struct Mol. Biol. 2009, 16 (6), 574-601
- (10) Ke, P. C.; Zhou, R.; Serpell, L. C.; Riek, R.; Knowles, T. P. J.; 603 Lashuel, H. A.; Gazit, E.; Hamley, I. W.; Davis, T. P.; Fändrich, M.; 604

- 605 Otzen, D. E.; Chapman, M. R.; Dobson, C. M.; Eisenberg, D. S.; 606 Mezzenga, R. Half a century of amyloids: past, present and future. 607 Chem. Soc. Rev. 2020, 49 (15), 5473–5509.
- 608 (11) Terzi, E.; Hölzemann, G.; Seelig, J. Interaction of Alzheimer 609 beta-amyloid peptide(1–40) with lipid membranes. *Biochemistry* 610 **1997**, *36* (48), 14845–52.
- 611 (12) Robinson, P. J.; Pinheiro, T. J. Phospholipid composition of 612 membranes directs prions down alternative aggregation pathways. 613 *Biophys. J.* **2010**, *98* (8), 1520–8.
- 614 (13) Galvagnion, C.; Buell, A. K.; Meisl, G.; Michaels, T. C.; 615 Vendruscolo, M.; Knowles, T. P.; Dobson, C. M. Lipid vesicles trigger 616 α -synuclein aggregation by stimulating primary nucleation. *Nat. Chem.* 617 *Biol.* **2015**, *11* (3), 229–34.
- 618 (14) Grigolato, F.; Arosio, P. The role of surfaces on amyloid 619 formation. *Biophys Chem.* **2021**, 270, No. 106533.
- 620 (15) McLaurin, J.; Franklin, T.; Zhang, X.; Deng, J.; Fraser, P. E. 621 Interactions of Alzheimer amyloid-beta peptides with glycosamino-622 glycans effects on fibril nucleation and growth. *Eur. J. Biochem.* 1999, 623 266 (3), 1101–10.
- 624 (16) Snow, A. D.; Wight, T. N. Proteoglycans in the pathogenesis of 625 Alzheimer's disease and other amyloidoses. *Neurobiol Aging* **1989**, *10* 626 (5), 481–97.
- 627 (17) Rahman, M. M.; Lendel, C. Extracellular protein components 628 of amyloid plaques and their roles in Alzheimer's disease pathology. 629 *Mol. Neurodegener.* **2021**, *16* (1), 59.
- 630 (18) Stege, G. J.; Renkawek, K.; Overkamp, P. S.; Verschuure, P.; 631 van Rijk, A. F.; Reijnen-Aalbers, A.; Boelens, W. C.; Bosman, G. J.; de 632 Jong, W. W. The molecular chaperone alphaB-Crystallin enhances 633 amyloid beta neurotoxicity. *Biochem. Biophys. Res. Commun.* 1999, 262 634 (1), 152–6.
- 635 (19) Wilson, M. R.; Yerbury, J. J.; Poon, S. Potential roles of 636 abundant extracellular chaperones in the control of amyloid formation 637 and toxicity. *Mol. Biosyst* **2008**, *4* (1), 42–52.
- 638 (20) Wright, M. A.; Aprile, F. A.; Arosio, P.; Vendruscolo, M.; 639 Dobson, C. M.; Knowles, T. P. J. Biophysical approaches for the study 640 of interactions between molecular chaperones and protein aggregates. 641 *Chem. Commun.* **2015**, *51* (77), 14425–14434.
- 642 (21) Arosio, P.; Michaels, T. C. T.; Linse, S.; Månsson, C.; 643 Emanuelsson, C.; Presto, J.; Johansson, J.; Vendruscolo, M.; Dobson, 644 C. M.; Knowles, T. P. J. Kinetic analysis reveals the diversity of 645 microscopic mechanisms through which molecular chaperones 646 suppress amyloid formation. *Nat. Commun.* **2016**, *7*, 10948.
- 647 (22) Linse, S. Mechanism of amyloid protein aggregation and the 648 role of inhibitors. *Pure Appl. Chem.* **2019**, *91* (2), 211–229.
- 649 (23) Sun, Y.; MacRae, T. H. The small heat shock proteins and their 650 role in human disease. Febs j 2005, 272 (11), 2613–27.
- 651 (24) Muchowski, P. J.; Wacker, J. L. Modulation of neuro-652 degeneration by molecular chaperones. *Nat. Rev. Neurosci* **2005**, 6653 (1), 11–22.
- 654 (25) Wilhelmus, M. M.; Otte-Höller, I.; Wesseling, P.; de Waal, R. 655 M.; Boelens, W. C.; Verbeek, M. M. Specific association of small heat 656 shock proteins with the pathological hallmarks of Alzheimer's disease 657 brains. *Neuropathol Appl. Neurobiol* **2006**, 32 (2), 119–30.
- 658 (26) Wilhelmus, M. M.; Boelens, W. C.; Otte-Höller, I.; Kamps, B.; 659 de Waal, R. M.; Verbeek, M. M. Small heat shock proteins inhibit 660 amyloid-beta protein aggregation and cerebrovascular amyloid-beta 661 protein toxicity. *Brain Res.* **2006**, *1089* (1), 67–78.
- 662 (27) Dehle, F. C.; Ecroyd, H.; Musgrave, I. F.; Carver, J. A. αB-663 Crystallin inhibits the cell toxicity associated with amyloid fibril 664 formation by κ -casein and the amyloid- β peptide. *Cell Stress* 665 *Chaperones* **2010**, *15* (6), 1013–26.
- 666 (28) Hochberg, G. K. A.; Ecroyd, H.; Liu, C.; Cox, D.; Cascio, D.;
 667 Sawaya, M. R.; Collier, M. P.; Stroud, J.; Carver, J. A.; Baldwin, A. J.;
 668 Robinson, C. V.; Eisenberg, D. S.; Benesch, J. L. P.; Laganowsky, A.
 669 The structured core domain of αB-Crystallin can prevent amyloid
 670 fibrillation and associated toxicity. *Proc. Natl. Acad. Sci. U. S. A.* 2014,
 671 111 (16), E1562–E1570.

- (29) Arosio, P.; Knowles, T. P. J.; Linse, S. On the lag phase in 672 amyloid fibril formation. *Phys. Chem. Chem. Phys.* **2015**, *17* (12), 673 7606–7618.
- (30) Chuang, E.; Hori, A. M.; Hesketh, C. D.; Shorter, J. Amyloid 675 assembly and disassembly. *J. Cell Sci.* **2018**, *131* (8), jcs189928.
- (31) Törnquist, M.; Michaels, T. C. T.; Sanagavarapu, K.; Yang, X.; 677 Meisl, G.; Cohen, S. I. A.; Knowles, T. P. J.; Linse, S. Secondary 678 nucleation in amyloid formation. *Chem. Commun.* **2018**, 54 (63), 679 8667–8684.
- (32) Louros, N.; Schymkowitz, J.; Rousseau, F. Mechanisms and 681 pathology of protein misfolding and aggregation. *Nat. Rev. Mol. Cell* 682 *Biol.* 2023, 24 (12), 912–933.
- (33) Cohen, S. I.; Linse, S.; Luheshi, L. M.; Hellstrand, E.; White, D. 684 A.; Rajah, L.; Otzen, D. E.; Vendruscolo, M.; Dobson, C. M.; 685 Knowles, T. P. Proliferation of amyloid-β42 aggregates occurs through 686 a secondary nucleation mechanism. *Proc. Natl. Acad. Sci. U. S. A.* 687 **2013**, 110 (24), 9758–63.
- (34) Thacker, D.; Barghouth, M.; Bless, M.; Zhang, E.; Linse, S. 689 Direct observation of secondary nucleation along the fibril surface of 690 the amyloid β 42 peptide. *Proc. Natl. Acad. Sci.* **2023**, *120*, 691 No. e2220664120.
- (35) Peduzzo, A.; Linse, S.; Buell, A. K. The Properties of α 693 Synuclein Secondary Nuclei Are Dominated by the Solution 694 Conditions Rather than the Seed Fibril Strain. *American Chemical* 695 Society: ACS Chem. Neurosci **2020**, 11, 909–918.
- (36) Hadi Alijanvand, S.; Peduzzo, A.; Buell, A. K. Secondary 697 Nucleation and the Conservation of Structural Characteristics of 698 Amyloid Fibril Strains. *Front Mol. Biosci* **2021**, 8, No. 669994.
- (37) Frey, L.; Ghosh, D.; Qureshi, B. M.; Rhyner, D.; Guerrero- 700 Ferreira, R.; Pokharna, A.; Kwiatkowski, W.; Serdiuk, T.; Picotti, P.; 701 Riek, R.; Greenwald, J. On the pH-dependence of α -synuclein 702 amyloid polymorphism and the role of secondary nucleation in seed- 703 based amyloid propagation. bioRxiv 2023, 2023-06.
- (38) Thacker, D.; Sanagavarapu, K.; Frohm, B.; Meisl, G.; Knowles, 705 T. P. J.; Linse, S. The role of fibril structure and surface 706 hydrophobicity in secondary nucleation of amyloid fibrils. *Proc.* 707 *Natl. Acad. Sci. U. S. A.* **2020**, *117* (41), 25272–25283.
- (39) Yang, X.; Wang, B.; Hoop, C. L.; Williams, J. K.; Baum, J. NMR 709 unveils an N-terminal interaction interface on acetylated-α-synuclein 710 monomers for recruitment to fibrils. *Proc. Natl. Acad. Sci. U S A* **2021**, 711 118, No. e2017452118.
- (40) Khare, S. D.; Chinchilla, P.; Baum, J. Multifaceted interactions 713 mediated by intrinsically disordered regions play key roles in alpha 714 synuclein aggregation. *Curr. Opin Struct Biol.* **2023**, 80, No. 102579. 715
- (41) Scheidt, T.; Łapińska, U.; Kumita, J. R.; Whiten, D. R.; 716 Klenerman, D.; Wilson, M. R.; Cohen, S. I. A.; Linse, S.; Vendruscolo, 717 M.; Dobson, C. M.; Knowles, T. P. J.; Arosio, P. Secondary nucleation 718 and elongation occur at different sites on Alzheimer's amyloid- β 719 aggregates. *Sci. Adv.* **2019**, 5 (4), No. eaau3112.
- (42) Cohen, S. I. A.; Arosio, P.; Presto, J.; Kurudenkandy, F. R.; 721 Biverstal, H.; Dolfe, L.; Dunning, C.; Yang, X.; Frohm, B.; 722 Vendruscolo, M.; Johansson, J.; Dobson, C. M.; Fisahn, A.; 723 Knowles, T. P. J.; Linse, S. A molecular chaperone breaks the 724 catalytic cycle that generates toxic $A\beta$ oligomers. *Nat. Struct Mol. Biol.* 725 **2015**, 22 (3), 207–213.
- (43) Kumar, R.; Le Marchand, T.; Adam, L.; Bobrovs, R.; Chen, G.; 727 Fridmanis, J.; Kronqvist, N.; Biverstål, H.; Jaudzems, K.; Johansson, J.; 728 Pintacuda, G.; Abelein, A. Identification of potential aggregation 729 hotspots on $A\beta$ 42 fibrils blocked by the anti-amyloid chaperone-like 730 BRICHOS domain. *Nat. Commun.* **2024**, *15* (1), 965.
- (44) Aprile, F. A.; Arosio, P.; Fusco, G.; Chen, S. W.; Kumita, J. R.; 732 Dhulesia, A.; Tortora, P.; Knowles, T. P.; Vendruscolo, M.; Dobson, 733 C. M.; Cremades, N. Inhibition of α -Synuclein Fibril Elongation by 734 Hsp70 Is Governed by a Kinetic Binding Competition between α 735 Synuclein Species. *Biochemistry* **2017**, 56 (9), 1177–1180.
- (45) Cox, D.; Whiten, D. R.; Brown, J. W. P.; Horrocks, M. H.; San 737 Gil, R.; Dobson, C. M.; Klenerman, D.; van Oijen, A. M.; Ecroyd, H. 738 The small heat shock protein Hsp27 binds α-synuclein fibrils, 739

- 740 preventing elongation and cytotoxicity. *J. Biol. Chem.* **2018**, 293 (12), 741 4486–4497.
- 742 (46) Österlund, N.; Frankel, R.; Carlsson, A.; Thacker, D.; Karlsson, 743 M.; Matus, V.; Gräslund, A.; Emanuelsson, C.; Linse, S. The C-744 terminal domain of the antiamyloid chaperone DNAJB6 binds to 745 amyloid-β peptide fibrils and inhibits secondary nucleation. *J. Biol.* 746 *Chem.* **2023**, 299 (11), No. 105317.
- 747 (47) Waudby, C. A.; Knowles, T. P.; Devlin, G. L.; Skepper, J. N.; 748 Ecroyd, H.; Carver, J. A.; Welland, M. E.; Christodoulou, J.; Dobson, 749 C. M.; Meehan, S. The interaction of alphaB-Crystallin with mature 750 alpha-synuclein amyloid fibrils inhibits their elongation. *Biophys. J.* 751 **2010**, 98 (5), 843–51.
- 752 (48) Shammas, S. L.; Waudby, C. A.; Wang, S.; Buell, A. K.; 753 Knowles, T. P. J.; Ecroyd, H.; Welland, M. E.; Carver, J. A.; Dobson, 754 C. M.; Meehan, S. Binding of the Molecular Chaperone α B-Crystallin 755 to $A\beta$ Amyloid Fibrils Inhibits Fibril Elongation. *Biophys. J.* **2011**, *101*, 756 1681–1689.
- 757 (49) Scheidt, T.; Carozza, J. A.; Kolbe, C. C.; Aprile, F. A.; 758 Tkachenko, O.; Bellaiche, M. M. J.; Meisl, G.; Peter, Q. A. E.; Herling, 759 T. W.; Ness, S.; Castellana-Cruz, M.; Benesch, J. L. P.; Vendruscolo, 760 M.; Dobson, C. M.; Arosio, P.; Knowles, T. P. J. The binding of the 761 small heat-shock protein α B-Crystallin to fibrils of α -synuclein is 762 driven by entropic forces. *Proc. Natl. Acad. Sci. U. S. A.* **2021**, *118* 763 (38), No. e2108790118.
- 764 (50) Mainz, A.; Peschek, J.; Stavropoulou, M.; Back, K. C.; Bardiaux, 765 B.; Asami, S.; Prade, E.; Peters, C.; Weinkauf, S.; Buchner, J.; Reif, B. 766 The chaperone α B-Crystallin uses different interfaces to capture an 767 amorphous and an amyloid client. *Nat. Struct Mol. Biol.* **2015**, 22 (11), 768 898–905.
- 769 (51) Lopez del Amo, J. M.; Schmidt, M.; Fink, U.; Dasari, M.; 770 Fändrich, M.; Reif, B. An asymmetric dimer as the basic subunit in 771 Alzheimer's disease amyloid β fibrils. *Angew. Chem., Int. Ed. Engl.* 772 **2012,** 51 (25), 6136–9.
- 773 (52) van Helmond, Z.; Miners, J. S.; Kehoe, P. G.; Love, S. Higher 774 soluble amyloid beta concentration in frontal cortex of young adults 775 than in normal elderly or Alzheimer's disease. *Brain Pathol* **2010**, *20* 776 (4), 787–93.
- 777 (53) Wang, Z.; Jin, M.; Hong, W.; Liu, W.; Reczek, D.; Lagomarsino, 778 V. N.; Hu, Y.; Weeden, T.; Frosch, M. P.; Young-Pearse, T. L.; 779 Pradier, L.; Selkoe, D.; Walsh, D. M. Learnings about $A\beta$ from human 780 brain recommend the use of a live-neuron bioassay for the discovery 781 of next generation Alzheimer's disease immunotherapeutics. *Acta Neuropathol. Commun.* **2023**, *11* (1), 39.
- 783 (54) Shinohara, H.; Inaguma, Y.; Goto, S.; Inagaki, T.; Kato, K. 784 Alpha B Crystallin and HSP28 are enhanced in the cerebral cortex of 785 patients with Alzheimer's disease. *J. Neurol Sci.* **1993**, *119* (2), 203–8. 786 (55) Micsonai, A.; Wien, F.; Kernya, L.; Lee, Y. H.; Goto, Y.; 787 Réfrégiers, M.; Kardos, J. Accurate secondary structure prediction and 788 fold recognition for circular dichroism spectroscopy. *Proc. Natl. Acad.* 789 *Sci. U. S. A.* **2015**, *112* (24), E3095.
- 790 (56) Tycko, R. Molecular Structure of Aggregated Amyloid- β : 791 Insights from Solid-State Nuclear Magnetic Resonance. *Cold Spring* 792 *Harbor Perspect. Med.* **2016**, 6 (8), a024083.
- 793 (57) Xiao, Y.; Ma, B.; McElheny, D.; Parthasarathy, S.; Long, F.; 794 Hoshi, M.; Nussinov, R.; Ishii, Y. $A\beta(1-42)$ fibril structure 795 illuminates self-recognition and replication of amyloid in Alzheimer's 796 disease. *Nat. Struct Mol. Biol.* **2015**, 22 (6), 499–505.
- 797 (58) Sgourakis, N. G.; Yau, W. M.; Qiang, W. Modeling an in-798 register, parallel "iowa" a β fibril structure using solid-state NMR data 799 from labeled samples with rosetta. *Structure* **2015**, 23 (1), 216–227. 800 (59) Ulamec, S. M.; Brockwell, D. J.; Radford, S. E. Looking beyond 801 the core: the role of flanking regions in the aggregation of 802 amyloidogenic peptides and proteins. *Frontiers in Neuroscience* **2020**, 803 14, No. 611285.
- 804 (60) Khare, S. D.; Chinchilla, P.; Baum, J. Multifaceted interactions 805 mediated by intrinsically disordered regions play key roles in alpha 806 synuclein aggregation. *Curr. Opin. Struct. Biol.* **2023**, *80*, No. 102579. 807 (61) Yang, Y.; Arseni, D.; Zhang, W.; Huang, M.; Lövestam, S.; 808 Schweighauser, M.; Kotecha, A.; Murzin, A. G.; Peak-Chew, S. Y.;

- Macdonald, J.; Lavenir, I.; Garringer, H. J.; Gelpi, E.; Newell, K. L.; 809 Kovacs, G. G.; Vidal, R.; Ghetti, B.; Ryskeldi-Falcon, B.; Scheres, S. H. 810 W.; Goedert, M. Cryo-EM structures of amyloid- β 42 filaments from 811 human brains. *Science* **2022**, 375 (6577), 167–172.
- (62) Milanesi, M.; Faidon Brotzakis, Z.; Vendruscolo, M. Transient 813 interactions between the fuzzy coat and the cross- β core of brain- 814 derived A β 42 filaments. *bioRxiv* **2024**, 2024-01.
- (63) Abelein, A.; Jarvet, J.; Barth, A.; Gräslund, A.; Danielsson, J. 816 Ionic Strength Modulation of the Free Energy Landscape of $A\beta$ 40 817 Peptide Fibril Formation. *J. Am. Chem. Soc.* **2016**, *138* (21), 6893–818 6902.
- (64) Meisl, G.; Yang, X.; Dobson, C. M.; Linse, S.; Knowles, T. P. J. 820 Modulation of electrostatic interactions to reveal a reaction network 821 unifying the aggregation behaviour of the $A\beta$ 42 peptide and its 822 variants. *Chem. Sci.* **2017**, 8 (6), 4352–4362.
- (65) Cohen, S. I. A.; Cukalevski, R.; Michaels, T. C. T.; Šarić, A.; 824 Törnquist, M.; Vendruscolo, M.; Dobson, C. M.; Buell, A. K.; 825 Knowles, T. P. J.; Linse, S. Distinct thermodynamic signatures of 826 oligomer generation in the aggregation of the amyloid- β peptide. *Nat.* 827 *Chem.* 2018, 10 (5), 523–531.
- (66) Jarrett, J. T.; Lansbury, P. T., Jr. Seeding "one-dimensional 829 crystallization" of amyloid: a pathogenic mechanism in Alzheimer's 830 disease and scrapie? *Cell* **1993**, *73* (6), 1055–8.
- (67) Jucker, M.; Walker, L. C. Self-propagation of pathogenic 832 protein aggregates in neurodegenerative diseases. *Nature* **2013**, *501* 833 (7465), 45–51.
- (68) Spirig, T.; Ovchinnikova, O.; Vagt, T.; Glockshuber, R. Direct 835 evidence for self-propagation of different amyloid- β fibril conformations. *Neurodegener Dis* **2014**, *14* (3), 151–9.
- (69) Radamaker, L.; Baur, J.; Huhn, S.; Haupt, C.; Hegenbart, U.; 838 Schönland, S.; Bansal, A.; Schmidt, M.; Fändrich, M. Cryo-EM reveals 839 structural breaks in a patient-derived amyloid fibril from systemic AL 840 amyloidosis. *Nat. Commun.* **2021**, *12* (1), 875.
- (70) Lövestam, S.; Schweighauser, M.; Matsubara, T.; Murayama, S.; 842 Tomita, T.; Ando, T.; Hasegawa, K.; Yoshida, M.; Tarutani, A.; 843 Hasegawa, M.; Goedert, M.; Scheres, S. H. W. Seeded assembly in 844 vitro does not replicate the structures of α -synuclein filaments from 845 multiple system atrophy. *FEBS Open Bio* **2021**, *11* (4), 999–1013. 846
- (71) LeVine, H., 3rd Thioflavine T interaction with amyloid-sheet 847 structures. *Amyloid: Int. J. Exp. Clin. Invest.* **1995**, 2, 1–6. 848
- (72) Voropai, E. S.; Samtsov, M. P.; Kaplevskii, K. N.; Maskevich, A. 849 A.; Stepuro, V. I.; Povarova, O. I.; Kuznetsova, I. M.; Turoverov, K. 850 K.; Fink, A. L.; Uverskii, V. N. Spectral Properties of Thioflavin T and 851 Its Complexes with Amyloid Fibrils. *J. Appl. Spectrosc.* **2003**, 70 (6), 852 868–874
- (73) Sulatskaya, A. I.; Kuznetsova, I. M.; Turoverov, K. K. 854 Interaction of thioflavin T with amyloid fibrils: fluorescence quantum 855 yield of bound dye. *J. Phys. Chem. B* **2012**, *116* (8), 2538–44.
- (74) Sulatskaya, A. I.; Rodina, N. P.; Polyakov, D. S.; Sulatsky, M. I.; 857 Artamonova, T. O.; Khodorkovskii, M. A.; Shavlovsky, M. M.; 858 Kuznetsova, I. M.; Turoverov, K. K. Structural Features of Amyloid 859 Fibrils Formed from the Full-Length and Truncated Forms of Beta-2-860 Microglobulin Probed by Fluorescent Dye Thioflavin T. *Int. J. Mol.* 861 *Sci.* 2018, 19 (9), 6411.
- (75) Sulatskaya, A. I.; Rodina, N. P.; Sulatsky, M. I.; Povarova, O. I.; 863 Antifeeva, I. A.; Kuznetsova, I. M.; Turoverov, K. K. Investigation of 864 α -Synuclein Amyloid Fibrils Using the Fluorescent Probe Thioflavin 865 T. *Int. J. Mol. Sci.* **2018**, 19 (9), 2486.
- (76) Sulatsky, M. I.; Sulatskaya, A. I.; Povarova, O. I.; Antifeeva, I. 867 A.; Kuznetsova, I. M.; Turoverov, K. K. Effect of the fluorescent 868 probes ThT and ANS on the mature amyloid fibrils. *Prion* **2020**, 14 869 (1), 67–75.
- (77) Groenning, M.; Olsen, L.; van de Weert, M.; Flink, J. M.; 871 Frokjaer, S.; Jorgensen, F. S. Study on the binding of Thioflavin T to 872 beta-sheet-rich and non-beta-sheet cavities. *J. Struct. Biol.* **2007**, *158* 873 (3), 358–69.
- (78) Groenning, M.; Norrman, M.; Flink, J. M.; van de Weert, M.; 875 Bukrinsky, J. T.; Schluckebier, G.; Frokjaer, S. Binding mode of 876

- 877 Thioflavin T in insulin amyloid fibrils. *J. Struct. Biol.* **200**7, *159* (3), 878 483–97.
- 879 (79) Yoshiike, Y.; Akagi, T.; Takashima, A. Surface structure of 880 amyloid-beta fibrils contributes to cytotoxicity. *Biochemistry* **2007**, 46 881 (34), 9805–12.
- 882 (80) Xue, W. F.; Hellewell, A. L.; Gosal, W. S.; Homans, S. W.; 883 Hewitt, E. W.; Radford, S. E. Fibril Fragmentation Enhances Amyloid 884 Cytotoxicity. *American Society for Biochemistry and Molecular Biology:* 885 *J. Biol. Chem.* **2009**, 284, 34272–82.
- 886 (81) Xue, W.-F.; Hellewell, A. L.; Hewitt, E. W.; Radford, S. E. Fibril 887 fragmentation in amyloid assembly and cytotoxicity: When size 888 matters. *Taylor & Francis: Prion* **2010**, *4*, 20–25.
- 889 (82) Marshall, K. E.; Marchante, R.; Xue, W. F.; Serpell, L. C. The 890 relationship between amyloid structure and cytotoxicity. *Prion* **2014**, 8 891 (2), 192–6.
- 892 (83) Korn, A.; McLennan, S.; Adler, J.; Krueger, M.; Surendran, D.; 893 Maiti, S.; Huster, D. Amyloid β (1–40) Toxicity Depends on the 894 Molecular Contact between Phenylalanine 19 and Leucine 34. ACS 895 Chem. Neurosci. 2018, 9 (4), 790–799.
- 896 (84) Schwarze, B.; Korn, A.; Höfling, C.; Zeitschel, U.; Krueger, M.; 897 Roßner, S.; Huster, D. Peptide backbone modifications of amyloid β 898 (1–40) impact fibrillation behavior and neuronal toxicity. *Sci. Rep.* 899 **2021**, *11* (1), 23767.
- 900 (85) Hertel, C.; Terzi, E.; Hauser, N.; Jakob-Rotne, R.; Seelig, J.; 901 Kemp, J. A. Inhibition of the electrostatic interaction between beta-902 amyloid peptide and membranes prevents beta-amyloid-induced 903 toxicity. *Proc. Natl. Acad. Sci. U. S. A.* 1997, 94 (17), 9412–6.
- 904 (86) Anderson, K. L.; Ferreira, A. alpha1 Integrin activation: a link 905 between beta-amyloid deposition and neuronal death in aging 906 hippocampal neurons. *J. Neurosci Res.* **2004**, *75* (5), 688–97.
- 907 (87) Chi, E. Y.; Frey, S. L.; Lee, K. Y. Ganglioside G(M1)-mediated 908 amyloid-beta fibrillogenesis and membrane disruption. *Biochemistry* 909 **200**7, 46 (7), 1913–24.
- 910 (88) Han, H. Y.; Zhang, J. P.; Ji, S. Q.; Liang, Q. M.; Kang, H. C.; 911 Tang, R. H.; Zhu, S. Q.; Xue, Z. $\alpha\nu$ and β 1 Integrins mediate A β -912 induced neurotoxicity in hippocampal neurons via the FAK signaling 913 pathway. *PLoS One* **2013**, *8* (6), No. e64839.
- 914 (89) Shi, J.-M.; Li, H.-Y.; Liu, H.; Zhu, L.; Guo, Y.-B.; Pei, J.; An, H.; 915 Li, Y.-S.; Li, S.-D.; Zhang, Z.-Y.; Zheng, Y. N-terminal Domain of 916 Amyloid- β Impacts Fibrillation and Neurotoxicity. *ACS Omega* **2022**, 917 7 (43), 38847–38855.
- 918 (90) Venkatasubramaniam, A.; Drude, A.; Good, T. Role of N-919 terminal residues in $A\beta$ interactions with integrin receptor and cell 920 surface. *Biochimica et Biophysica Acta (BBA) - Biomembranes* **2014**, 921 1838 (10), 2568–2577.
- 922 (91) Narayanan, S.; Kamps, B.; Boelens, W. C.; Reif, B. α B-923 Crystallin competes with Alzheimer's disease β -amyloid peptide for 924 peptide—peptide interactions and induces oxidation of Abeta-Met35. 925 FEBS Lett. **2006**, 580, 5941—5946.
- 926 (92) Verma, M.; Vats, A.; Taneja, V. Toxic species in amyloid 927 disorders: Oligomers or mature fibrils. *Ann. Indian Acad. Neurol* **2015**, 928 18 (2), 138–45.
- 929 (93) Walsh, D. M.; Selkoe, D. J. A beta oligomers a decade of 930 discovery. *J. Neurochem* **2007**, *101* (5), 1172–84.
- 931 (94) Haass, C.; Selkoe, D. J. Soluble protein oligomers in 932 neurodegeneration: lessons from the Alzheimer's amyloid beta-933 peptide. *Nat. Rev. Mol. Cell Biol.* **2007**, *8* (2), 101–12.
- 934 (95) Sakono, M.; Zako, T. Amyloid oligomers: formation and 935 toxicity of Abeta oligomers. FEBS J. 2010, 277 (6), 1348-58.
- 936 (96) Huang, Y.-r.; Liu, R.-t. The Toxicity and Polymorphism of β -937 Amyloid Oligomers. *Int. J. Mol. Sci.* **2020**, 21 (12), 4477.
- 938 (97) Guo, L.; Giasson, B. I.; Glavis-Bloom, A.; Brewer, M. D.; 939 Shorter, J.; Gitler, A. D.; Yang, X. A cellular system that degrades 940 misfolded proteins and protects against neurodegeneration. *Mol. Cell* 941 **2014**, 55 (1), 15–30.
- 942 (98) Wang, H.; Saunders, A. J. The role of ubiquitin-proteasome in 943 the metabolism of amyloid precursor protein (APP): implications for 944 novel therapeutic strategies for Alzheimer's disease. *Discov Med.* **2014**, 945 *18* (97), 41–50.

- (99) Gao, X.; Carroni, M.; Nussbaum-Krammer, C.; Mogk, A.; 946 Nillegoda, N. B.; Szlachcic, A.; Guilbride, D. L.; Saibil, H. R.; Mayer, 947 M. P.; Bukau, B. Human Hsp70 Disaggregase Reverses Parkinson's- 948 Linked α -Synuclein Amyloid Fibrils. *Mol. Cell* **2015**, 59 (5), 781–93. 949 (100) Wentink, A. S.; Nillegoda, N. B.; Feufel, J.; Ubartaitė, G.; 950 Schneider, C. P.; De Los Rios, P.; Hennig, J.; Barducci, A.; Bukau, B. 951 Molecular dissection of amyloid disaggregation by human HSP70. 952 *Nature* **2020**, 587 (7834), 483–488.
- (101) Selig, E. E.; Zlatic, C. O.; Cox, D.; Mok, Y. F.; Gooley, P. R.; 954 Ecroyd, H.; Griffin, M. D. W. N- and C-terminal regions of α B- 955 Crystallin and Hsp27 mediate inhibition of amyloid nucleation, fibril 956 binding, and fibril disaggregation. *J. Biol. Chem.* **2020**, 295 (29), 957 9838–9854.
- (102) Selig, E. E.; Lynn, R. J.; Zlatic, C. O.; Mok, Y. F.; Ecroyd, H.; 959 Gooley, P. R.; Griffin, M. D. W. The Monomeric α -Crystallin Domain 960 of the Small Heat-shock Proteins α B-Crystallin and Hsp27 Binds 961 Amyloid Fibril Ends. *J. Mol. Biol.* **2022**, 434 (16), No. 167711. 962
- (103) Bendifallah, M.; Redeker, V.; Monsellier, E.; Bousset, L.; 963 Bellande, T.; Melki, R. Interaction of the chaperones alpha B- 964 Crystallin and CHIP with fibrillar alpha-synuclein: Effects on 965 internalization by cells and identification of interacting interfaces. 966 Biochem. Biophys. Res. Commun. 2020, 527 (3), 760–769.
- (104) Stepanenko, O. V.; Sulatsky, M. I.; Mikhailova, E. V.; 968 Stepanenko, O. V.; Povarova, O. I.; Kuznetsova, I. M.; Turoverov, K. 969 K.; Sulatskaya, A. I. Alpha-B-Crystallin Effect on Mature Amyloid 970 Fibrils: Different Degradation Mechanisms and Changes in 971 Cytotoxicity. *Int. J. Mol. Sci.* **2020**, 21, 7659.
- (105) Sulatsky, M. I.; Stepanenko, O. V.; Stepanenko, O. V.; 973 Mikhailova, E. V.; Kuznetsova, I. M.; Turoverov, K. K.; Sulatskaya, A. 974 I. Amyloid fibrils degradation: the pathway to recovery or aggravation 975 of the disease? *Front. Mol. Biosci.* **2023**, *10*, 1208059.
- (106) Stefani, M. Biochemical and biophysical features of both 977 oligomer/fibril and cell membrane in amyloid cytotoxicity. *Febs j* 978 **2010**, 277 (22), 4602–13.
- (107) Tipping, K. W.; Karamanos, T. K.; Jakhria, T.; Iadanza, M. G.; 980 Goodchild, S. C.; Tuma, R.; Ranson, N. A.; Hewitt, E. W.; Radford, S. 981 E. pH-induced molecular shedding drives the formation of amyloid 982 fibril-derived oligomers. *Proc. Natl. Acad. Sci. U. S. A.* **2015**, *112* (18), 983 5691–6.